RESEARCH ARTICLE

Micron track chitosan conduit fabricated by 3D-printed model topography provides bionic microenvironment for peripheral nerve regeneration

Meng Zhang[1†]**, Heng An**[2†]**, Teng Wan**[1]**, Hao-Ran Jiang**[1]**, Ming Yang**[1]***, Yong-Qiang Wen**[2]***, Pei-Xun Zhang**[1]*

[1]Department of Orthopedics and Trauma, Peking University People's Hospital, Key Laboratory of Trauma and Neural Regeneration, Peking University, National Center for Trauma Medicine, Beijing 100044, China

[2]Beijing Key Laboratory for Bioengineering and Sensing Technology, Daxing Research Institute, School of Chemistry & Biological Engineering, University of Science & Technology Beijing, Beijing 100083, China

(This article belongs to the *Special Issue: Additive Manufacturing of Functional Biomaterials*)

Abstract

The micron track conduit (MTC) and nerve factor provide a physical and biological model for simulating peripheral nerve growth and have potential applications for nerve injury. However, it has rarely been reported that they synergize on peripheral nerves. In this study, we used bioderived chitosan as a substrate to design and construct a neural repair conduit with micron track topography using three-dimensional (3D) printing topography. We loaded the MTC with neurotrophin-3 (NT-3) to promote the regeneration of sensory and sympathetic neurons in the peripheral nervous system. We found that the MTC@NT3 composite nerve conduit mimicked the microenvironment of peripheral nerves and promoted axonal regeneration while inducing the targeted growth of Schwann cells, which would promote functional recovery in rats with peripheral nerve injury. Artificial nerve implants with functional properties can be developed using the strategy presented in this study.

Keywords: 3D printing; Micron track conduit; Peripheral nerve regeneration; Neurotrophin-3; Long-distance injury

†These authors contributed equally to this work.

*Corresponding authors:
Ming Yang
(bdyangming@aliyun.com)

Yong-Qiang Wen
(wyq_wen@ustb.edu.cn)

Pei-Xun Zhang
(zhangpeixun@bjmu.edu.cn)

1. Introduction

The morbidity rate for peripheral nerve injury (PNI) is extremely high[1,2]. Traffic accidents, trauma, and iatrogenic causes are the most common causes of PNI[3]. Each year, approximately 1.6 billion USD is spent on the medical treatment of patients with PNI in the United States[4]. In comparison with the central nervous system (CNS), the peripheral nervous system (PNS) is more capable of spontaneous regeneration after injury due to the intrinsic growth capacity of neurons and the permissive microenvironment provided by Schwann cells (SCs), which are activated during an injury[5]. Regenerating peripheral nerves after injury is possible but is complicated and takes a long time. There has been considerable progress in the development of artificial nerve implants for the clinical

treatment of PNI using natural and synthetic biomaterials. Unfortunately, a significant amount of improvement is still needed to improve peripheral nerve function after surgical repair. The failure of artificial nerve conduits is attributed to the slow migration of cells and axons and the disorganized growth of new nerve tissue[6].

Treatment of long-distance nerve defects has optimally been done with autologous nerve grafting[7], particularly when direct end-to-end suturing is not feasible. There are a few limitations using autologous nerve grafting. First, there are only a limited number of sources of the donor's nerves, and the selection of a donor's nerve causes the denervation in the corresponding area. Second, clinical use of the donor's nerve is limited by its differences in dimensions from the injured nerve[8].

For a wide range of nerve regeneration applications, nerve conduits have become an alternative to autologous nerve grafts due to advancements in biomaterials and designs[9,10]. Many studies aim to promote peripheral nerve regeneration by increasing the conductivity of the conduit[11]. In light of this, more polymer-based functional nerve-guided conduits are being developed[12,13]. Furthermore, a variety of methods, including physical, chemical, and biological modifications, have been used over the last decade to modify nerve conduits by manipulating the factors that increase Schwann cell migration and axonal growth, such as surface charge, functional groups ($-NH_2$, $-COOH$), surface topography, growth factors, and proteins[14,15]. Surface topography plays an important role in guiding the contact of Schwann cells. Multiple studies have demonstrated that ordered tracks regulate Schwann cell proliferation, differentiation, and neuronal elongation direction[16,17]. They have found that Schwann cells migrate along nerve conduits with directional tracks, which provide the microenvironment for accurate nerve repair. In contrast, lack of an oriented topography may lead to random growth of nerve tissue and delay regeneration[9]. Electrostatic spinning, three-dimensional (3D) printing, and microneedle have been used to fabricate topographies such as ridge/groove structures, columnar fibers, or spherical structures on neural implants[18–23]. However, relatively few studies have shown how uniformly aligned micron tracks influence cell growth, differentiation, and neural regeneration[24]. According to several studies, the regeneration of neurons is affected by topology as a physical factor[25]. For example, PC12 cells can adhere and orient better to nanogrooved surfaces[26]. Micropatterns on polyester films modified with graphene oxide nanosheets promoted the migration of SCs in a directional direction[27]. In the report, SCs migrate fastest along stripes and have the strongest adhesion between cells. According to Omidinia-Anarkoli et al., grooved fibers facilitate synapse alignment, with neuronal axons extending maximally at 30–100 μm grooved fibers[28]. Micro-nano topologies have been demonstrated to effectively induce SC migration and orientation without affecting the original physiological functions of SCs by Yang et al.[29]. In addition, micron-topological track structures can regulate genes involved in myelin formation[30].

It has been found that physisorption or chemical cross-linking can immobilize many biomolecules on nerve conduits to accelerate nerve regeneration, including nerve growth factors, DNA, and peptides. These biomolecules, however, promote cell attachment and spreading but do not regulate cell migration or growth. Hence, the rapid proliferation of Schwann cells and directional axonal growth can be achieved by introducing both growth factors and micron tracks to make suitable nerve conduits.

In this study, a 3D-printed topology micron track conduit (MTC) was used to repair long-distance PNI with ridge/groove structures and special functional group ($-NH_2$, $-OH$) cues (Figure 1A). The physicochemical properties of the prepared hydrogels were investigated, including morphology and stress. Various topological cues and factor loading were examined in vitro to determine their synergistic effects on Schwann cell growth (Figure 1B). Interestingly, the MTC had good hemostatic and antimicrobial effects (Figure 1C and D). Additionally, we implanted this conduit into a 15-mm sciatic nerve defect in Sprague Dawley (SD) rats in order to systematically evaluate its effect on nerve regeneration (Figure 1E). To evaluate the effects of the treatment, morphological, immunofluorescence, and electrophysiological analyses were conducted. Furthermore, the CatWalk method was used to analyze muscle function. For the repair of long-segment peripheral nerve defects, the results of this study will provide an important experimental and theoretical basis. Peripheral nerve regeneration can be improved with the bionic microenvironmental scaffolds currently being developed.

2. Materials and methods

2.1. Materials
Chitosan (deacetylation degree 75–85%, molecular weight = 100,000), acetic acid, acetone, sodium hydroxide, methanol, and acetic anhydride are the products of MACKLIN. Phosphate-buffered saline (PBS) and dulbecco's modified eagle medium (DMEM) were purchased from Cytiva/Hyclone. Fetal bovine serum (FBS) was purchased from Serapro.

2.2. Fabrication of the MTC and MTC@NT3
One hundred and forty grams of 4% chitosan was added to 3500 ml of 2% acetic acid solution and stirred for 2 h until all the chitosan was dissolved and filtered through a
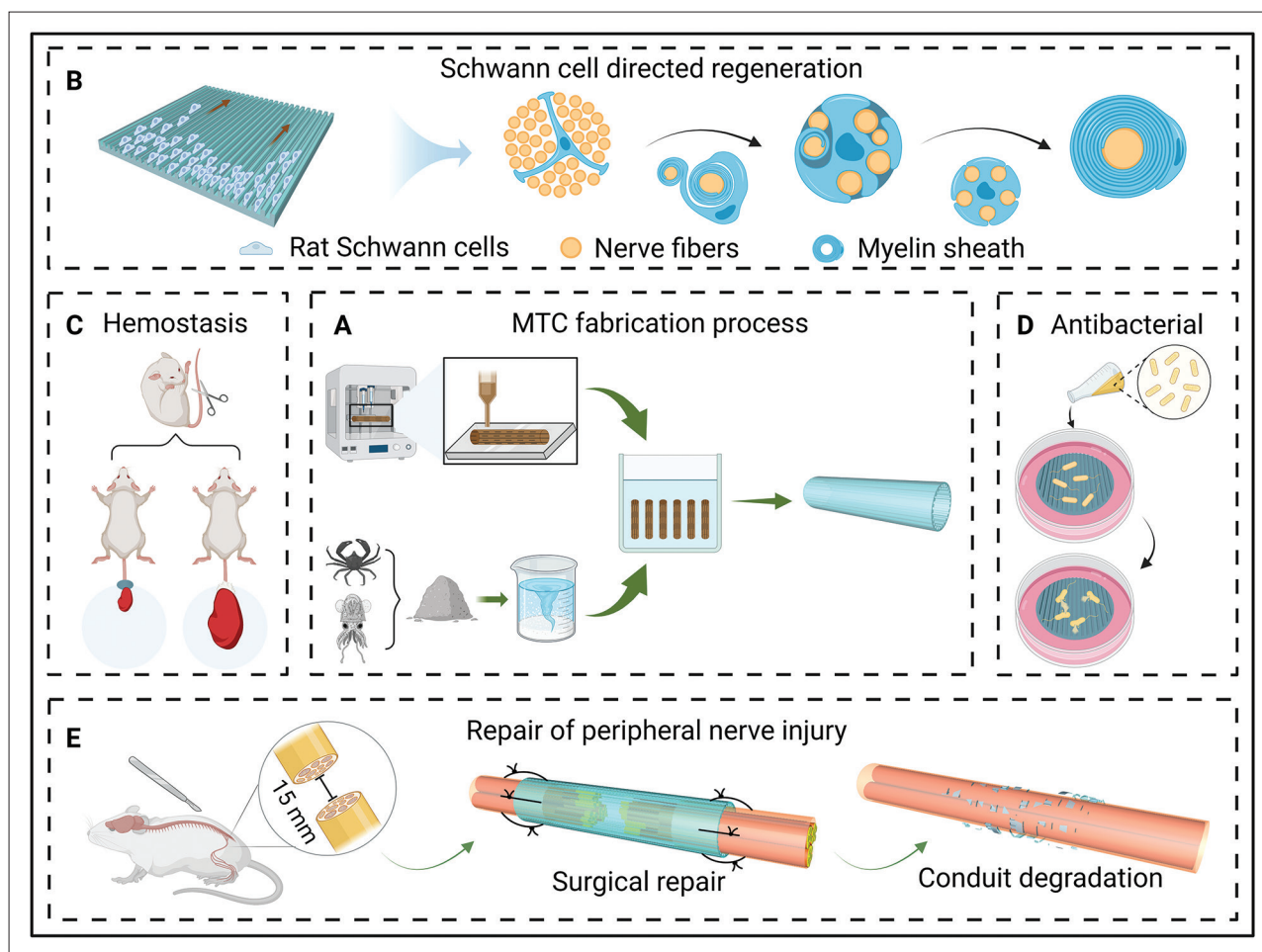
Figure 1. Fabrication and characterization of micron track conduit (MTC). (A) Fabrication of chitosan conduits by 3D printing topography. (B) MTC can promote Schwann cell-directed growth. (C) MTC has excellent hemostatic effect. (D) MTC has excellent antibacterial effect. (E) MTC promotes nerve regeneration and functional recovery from peripheral nerve injury.

20 μm diameter filter. As for the MTC@NT3 group, 10 μl of neurotrophin-3 (NT-3) was mixed into this solution and stirred. The upper layer solution was collected after one day of sonication. The 3SP™ E-Denstone Peach was printed by EnvisionTEC Micro Plus HD (Germany) into a mold with or without 30 μm ridges on the surface. The mold was immersed in chitosan solution, pulled out evenly, and immersed in 5% NaOH for 5 min. After soaking in deionized water overnight, it was dehydrated with acetone for 10 min. The chitosan conduit embedded with the mold was then immersed in a solution containing a 1:1 mixture of methanol and acetic anhydride for 5 min to fix it, and we could observe that the chitosan conduit became transparent. They were stored in 75% alcohol in a refrigerator at 4°C.

2.3. Morphological and mechanical evaluation of MTC and CC

The geometry, structural morphology, and structure of the prepared samples were characterized using a light microscope (Leica, Germany), a scanning electron microscope (Zeiss), and a surface morphometer (Zygo NewView 9000, USA). The dried samples were mounted on a measuring platform for optical microscopy observation. Three samples were photographed at the same angle, and the physical measurements were statistically analyzed on the acquired images. For observation with scanning electron microscopy (SEM), the samples were immersed in a fixative solution, followed by gradient dehydration in a series of increasing concentrations of alcohol. A layer of conductive material was deposited on the samples using a sputter coater, and the samples were placed in an SEM chamber where the electron beam was scanned over the surface of the samples at a magnification of 1000x. Finally, the surface and internal structure diagrams of MTC and commercial conduit (CC) were obtained. Tensile grips in tension mode were used to obtain stress–strain curves (MALK-10).

2.4. Cytocompatibility assay

To assess cytocompatibility, we cultured RSC96 cells (ATCC, CRL-2764) in a CO_2 incubator and then inoculated RSC96 onto sterilized MTC. After 1, 3, and 7 days of culture, RSC96 were stained using the LIVE/DEAD activity/cytotoxicity kit. Then, the viability and growth of RSC96 were analyzed by fluorescence images captured by inverted fluorescence microscopy (ZEISS), where live and dead cells were stained green and red, respectively.

2.5. Schwann cell's directed migration and proliferation

To evaluate the effect of MTC on the proliferation of primary Schwann cells (harvested from rat), we inoculated the isolated primary cells on sterilized MTC and placed them in a complete medium for culture. We stained with the Red Cell Chromatin Kit from Bestbio Biologics (product number: BB-441256). Nine photographs were randomly selected in $n > 3$ culture dishes to count the orientation angle to determine the Schwann cell's directed migration.

2.6. Hemolysis test

To test the hemocompatibility of MTC, 50, 100, and 200 μg of MTC samples were immersed in 1 ml of PBS, and rabbit red blood cells were added and incubated at 37°C to observe the extent of hemolysis. If the substance caused complete hemolysis, the tube would appear clear. If it caused partial hemolysis, the tube would appear cloudy.

2.7. Antibacterial experiment

To evaluate the antimicrobial properties of MTC, we prepared a bacterial culture. The bacteria were cultured on an agar plate until fully grown (*Escherichia coli*: ATCC 25922, *Staphylococcus aureus*, ATCC 6538). The MTC was cut into 5-mm diameter discs and placed on the surface of the agar plates, ensuring they were in contact with the bacterial cultures. The plates were incubated at 37°C for 1 and 3 days. The diameter of the clear area around the plate (i.e., the zone of inhibition) was measured using a ruler or caliper. The size of the inhibition zone is proportional to the antibacterial activity of the MTC. A larger inhibition zone indicates stronger antimicrobial activity, while a smaller inhibition zone or no zone of inhibition indicates weaker or no antimicrobial activity.

2.8. *In vivo* experiment

The rat sciatic nerve injury model is commonly used for studying nerve regeneration and repair. Rats were anesthetized, and a small incision was made in the skin of the lateral thigh. The sciatic nerve was then exposed, and the nerve was transected to create a 15-mm defect. After the injury, the wound was repaired with CC, MTC, MTC@NT3, or autologous nerve graft, respectively, and the wound was closed, and the rat was allowed to recover.

2.9. Immunofluorescence

The stained sections were used to identify and quantify the presence and distribution of regenerated axons in the peripheral nerve sections. The intensity and distribution of the NF200 staining indicated the degree of axonal regeneration, and the length and density of the stained axons provided information on the extent of nerve repair.

2.10. Toluidine blue stain

To assess the quality and quantity of regenerated myelin, we performed toluidine blue staining of tissue sections that were fixed and dehydrated. The sections were then stained with a toluidine blue solution that binds to the acidic components of the tissue, including the myelin sheath. The stained sections were then dehydrated and mounted for microscopic analysis.

2.11. Neurophysiological test

A neurophysiological test (NT) is a test that measures the speed of electrical signals traveling through the nerves. Electrodes were placed on the skin over the nerve being tested, and a small electric shock was applied. The speed and strength of the nerve's response to the shock were measured to determine if there was any nerve damage or dysfunction.

2.12. Gastrocnemius characterization

To test the maintenance of the target muscle in each group, we used MTC, CC, MTC@NT3, and autologous nerve graft (Autologous group) for peripheral nerve repair, respectively. After 8 and 12 weeks, the gastrocnemius muscle was harvested to measure the mean and cross-sectional areas, and Masson's staining was performed to obtain and analyze the data.

2.13. Sciatic function index

The Sciatic function index (SFI) is used to assess the degree of impairment of the sciatic nerve, the largest nerve in the body. The CatWalk instrument was used to test the calculated SFI (SFI = 109.5(ETS–NTS)/NTS–38.3(EPL–NPL)/NPL+13.3(EIT–NIT)/NIT–8.8) (N, normal foot; E, injured lateral foot; PL, footprint length; TS, toe width; IT, middle toe width).

2.14. Statistical analysis

The images obtained in this experiment were analyzed by ImageJ software. All numerical data were analyzed using Graph Prism Program, Version 7.0 (GraphPad Software, Inc., La Jolla, CA, USA) with mean ± SEM (Standard Error of Mean). Differences among multiple groups were analyzed by one-way analysis of variance (ANOVA). When $p > 0.05$, Tukey's *post hoc* test was applied in the

homogeneity of variances. Otherwise, Dunnett's T3 *post hoc* test was performed. In all analyses, $p < 0.05$ was considered statistically significant.

3. Results and discussion

3.1. MTC preparation and characterization
The MTC was fabricated by the 3D printing topography method, and the mold was made of 3SP™ E-Denstone Peach material (Figure 2A). Since the mold surface is hydrophobic, MTC was easily peeled off from its surface (**Figure S1** in Supplementary File). The acetic acid solution of chitosan was first dehydrated with acetone, then fixed with a mixture of methanol and acetic anhydride, and stored in 75% alcohol (Figure 2B). We used SEM to observe the fibrous pore structure of MTC (Figure 2C). Then, we measured the stress–strain curves of the CC and the MTC (Figure 2D) to obtain the mechanical information of the respective materials under load. The results showed that the MTC fabricated by 3D printing topography did not differ significantly from the CC in mechanical strength and was able to meet the basic strength of the peripheral nerve repair material.

The morphologies of MTC (Figure 2E) and CC (**Figure S2** in Supplementary File) were analyzed by SEM and surface morphometry, respectively. The results are shown in Figure 2F. It is clear that the MTC has 12 ± 3 μm ridges and 17 ± 4 μm grooves, showing a distinct orientation behavior. In addition, the flexibility and compressibility of the conduit proved to be excellent (**Figure S3** in Supplementary File). Furthermore, we performed a rat tail hemostasis experiment to observe the hemostatic effect of the MTC material (Figure 2G). Figure 2H shows that although cotton provided effective hemostasis, MTC had a higher hemostatic effect. In neurosurgery, hemostasis is very important because the hemostatic balance in the neurovascular unit affects peripheral nerve regeneration[31,32]. Especially in the presence of coagulopathies, nervous damage is exacerbated. It has been shown that the oriented spatial structure contributes to hemostasis[33,34]. Micron tracks on the inner surface of MTCs increased the contact area with blood clotting cells, thus influencing the blood clotting time.

3.2. Biocompatibility of the MTC
We further investigated the biological activity of MTC. Inoculating RSC96 cells on MTC and observing the staining using Calcein-AM/PI double Dead/Live cell staining kit[35,36], we found that RSC96 cells showed significant proliferation and no significant increase in dead cells after 1, 3, and 7 days (Figure 3A). To further confirm the effect of different concentrations of MTC leachate on cell growth[37], we found no significant difference from 0 to 5 mg/ml (Figure 3B). In addition, we performed a cell viability assay using RSC96 cells cultured on the materials as a model. We found that MTC and MTC@NT3 were able to support extremely high cell viability (>80%) over a 7-day culture period (Figure 3E), showing their excellent cytocompatibility. In comparison, there was no significant difference in biocompatibility between MTC and CC. MTC has excellent biocompatibility, which is essential for the development of implants.

### 3.3. Schwann cell's directed migration and proliferation
Schwann cells have been shown to play an important role in axon regeneration and maturation[38,39]. A higher growth density of primary Schwann cells was observed on MTC compared to CC[40] (Figure 3C). As shown in Figure 3D, the synaptic angle of Schwann cells cultured on MTC was mostly in the range of 70–110°, whereas Schwann cells on the CC grew irregularly. Thus, MTC helps to promote the rapid and directional growth of Schwann cells, providing the opportunity for axon growth and functional recovery. This phenomenon is inextricably linked to the guidance tracks on the inner surface of MTCs. It has been shown that the specific structure of the conduit material can influence the directional growth of Schwann cells[41–44].

3.4. Hemolytic and antibacterial properties of the materials
To test the effect of MTC on blood cells, we used rabbit erythrocytes co-cultured with different concentrations of MTC[45]. As shown in Figure 3F, the hemolysis ratio of MTC was not statistically different from the PBS group (negative control group) and was statistically significantly different from the water group (positive control group). In addition, as an implantable material, antimicrobial properties are critical[46]. By altering the 3D structure, many researchers have attempted to improve the antimicrobial properties of implants. We tested MTC against *Staphylococcus aureus* and *Escherichia coli* separately using the antimicrobial ring method, and the results showed significant antimicrobial effects similar to the CC (Figure 3G and H). This may be due to MTC increasing the specific surface area of the inner surface of chitosan, resulting in particularly high antimicrobial efficacy.

3.5. *In vivo* histologic evaluation
To evaluate the effect of MTC in promoting peripheral nerve regeneration in rats, we harvested the distal regenerated sciatic nerve of SD rats 8 weeks after repair surgery. By immunofluorescence staining with NF200 (Figure 4A) and S100 (**Figure S4** in Supplementary File)[47,48], we could see obvious neuromas in the CC group, which would probably cause a series of symptoms such as regenerative neuralgia (Figure 4A). In contrast, the MTC
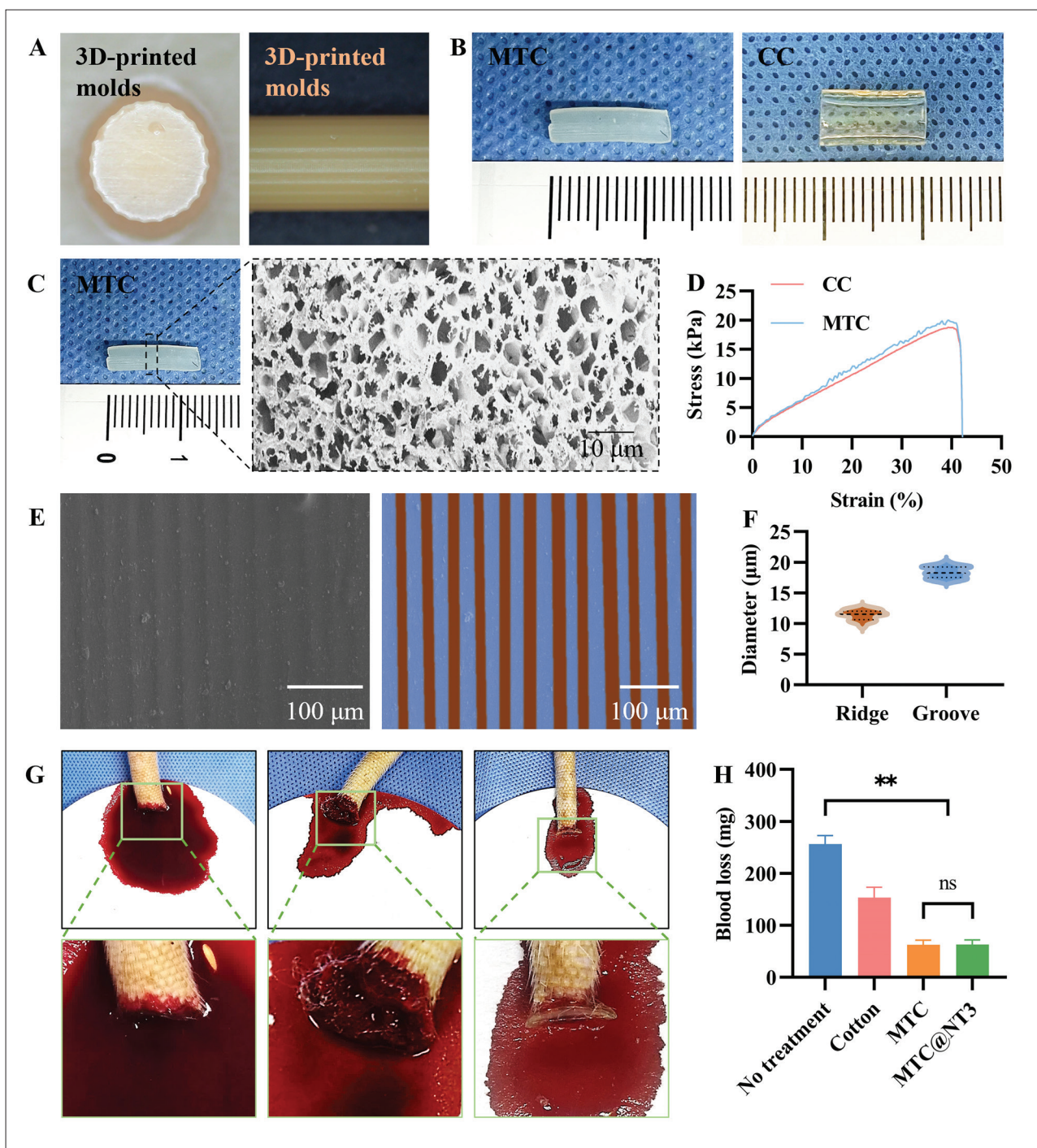
Figure 2. Microstructure and hemostatic effect of chitosan conduits. (A) 3D-printed mold with micron tracks. (B) The appearance of MTC and CC can be seen as a difference in the inner surface. (C) Electron microscopic microstructure of MTC. (D) Stress–strain curves of MTC and CC. (E) The topology of MTC was observed using scanning electron microscopy. The topology of MTC was observed using scanning electron microscopy and surface profile meter. (F) The widths of MTC micropatterns were statistically analyzed based on SEM images, respectively. (G) Rat tail hemostasis experiments of MTC. (H) Statistical results of the hemostatic response of MTC (ns = not significant, *$P < 0.05$, **$P < 0.01$).
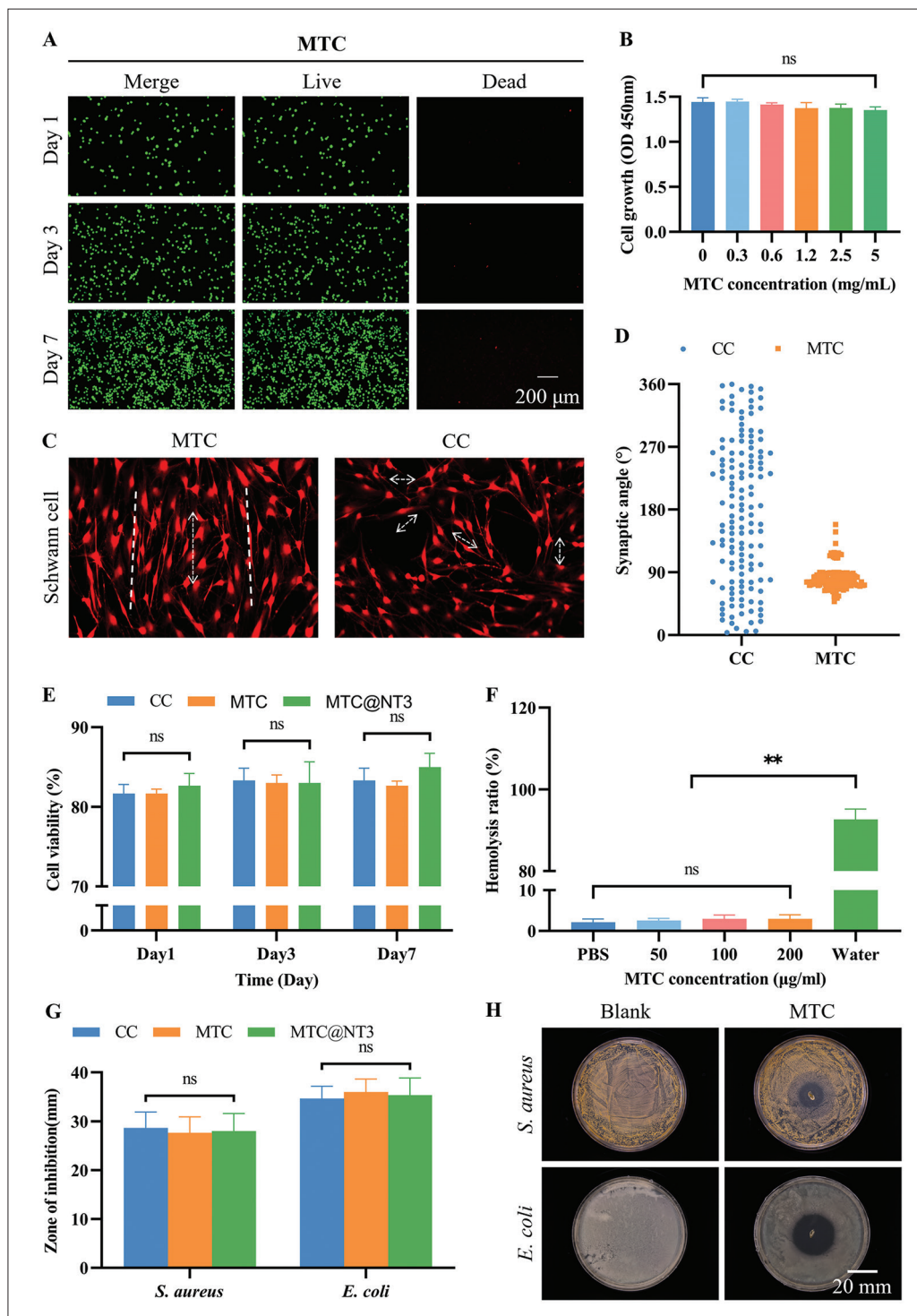
Figure 3. *In vitro* compatibility of MTC for orderly growth of Schwann cells and antimicrobial action. (A) Dead/Live of RSC96 cells on MTC using Calcein-AM/PI staining kit. (B) Effect of different concentrations of MTC leachate on cell growth. (C) Cytoplasmic staining to observe the topographical effect of MTC and CC (white arrow, the direction of Schwann cell axons) and on the growth of Schwann cells. (D) Distribution statistics of the synaptic angle of Schwann cells. (E) The activity of RSC96 cells on MTC at days 1, 3, and 7 was counted using CCK-8, respectively. (F) Absorbance assay was used to test the effect of different concentrations of MTC on the hemolysis of rabbit erythrocytes. (G, H) The antimicrobial effect of MTC against *S. aureus* and *E. coli* was tested using the inhibition ring method (ns = not significant, *$P < 0.05$, **$P < 0.01$).
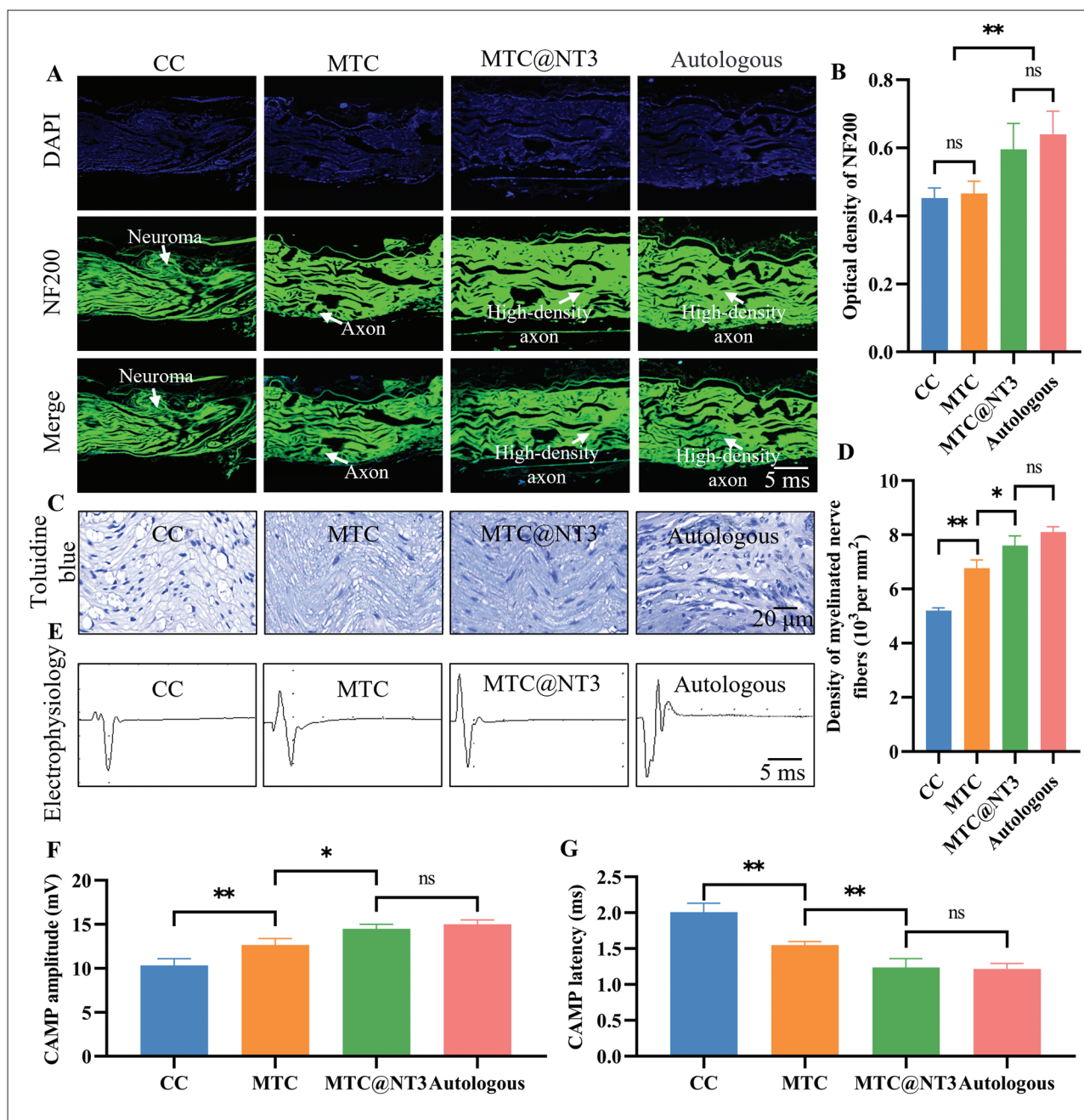
Figure 4. Histological characterization of peripheral nerve regeneration promoted by CC, MTC, MTC@NT3, and Autologous. (A) NF200 immunofluorescence staining to observe axonal regeneration. (B) The measured optical density of NF200 staining in the respective groups. (C) Toluidine blue staining of semithin sections showing nerve regeneration. (D) The counted density of myelinated nerve fibers in the respective groups. (E) Electrophysiological tests of regenerated nerves. (F, G) CAMP amplitude and CAMP latency statistics of regenerated nerves. (ns = not significant, $*P < 0.05$, $**P < 0.01$.)

group and the MTC@NT3 group had a higher density of axons, suggesting that the regenerated nerve had a better organization (**Figure S4** in Supplementary File). In addition, we also counted the visual density of regenerated axons in immunofluorescence staining using ImageJ. The results show no significant difference between the MTC

group and the CC group, while the MTC@NT3 group was able to promote the regeneration of axons more significantly (Figure 4B). In week 12, we saw a similar pattern (**Figure S6** in Supplementary File). Many studies have realized that Schwann cells and axons react as a unit and that changes in Schwann cells cause corresponding

changes in axons and vice versa[49]. In this work, the rapid directional migration of Schwann cells might provide scaffolding and protection from the misgrowth of nerve axons[50].

To further verify the ability of MTC to promote peripheral nerve regeneration, we stained nerve myelin with toluidine blue (Figure 4C). Figure 4D shows that the density of myelinated nerve fibers in MTC@NT3 was statistically higher than both the MTC and the CC groups and that the MTC group was statistically higher than the CC group, indicating that MTC was able to promote myelin regeneration. Since the myelin sheath of myelinated nerve fibers is mainly composed of Schwann cells, this result is consistent with Figure 3C.

We also evaluated the electrical conductivity of the regenerated nerves using neurophysiological instruments (Figure 4E). The results show that in terms of CAMP amplitude, the MTC@NT3 group was higher than the MTC and CC groups and was close to the Autologous group level (Figure 4F), and in terms of CAMP latency, the MTC group was shorter than the CC group, while the MTC@NT3 group was similar to the Autologous group (Figure 4G). This may be because NT3 promoted axonal regeneration and never had a higher amplitude of nerve electrical conduction. Moreover, the presence of micron tracks promoted the orderly regeneration of myelin, thus reducing the neuroelectric conduction delay. It is well known that the conduction velocity of myelinated nerve fibers is much higher than that of unmyelinated nerve fibers, and the degree of integrity of the myelin sheath greatly affects the electrical conduction performance of nerves[51,52]. By increasing myelin orientation and thickness, nerve conduction is moderately enhanced[53]. The difference in electrical conduction in regenerating nerves is mainly due to the directional and rapid growth of Schwann cells that wrap around nerve axons to form myelin sheaths.
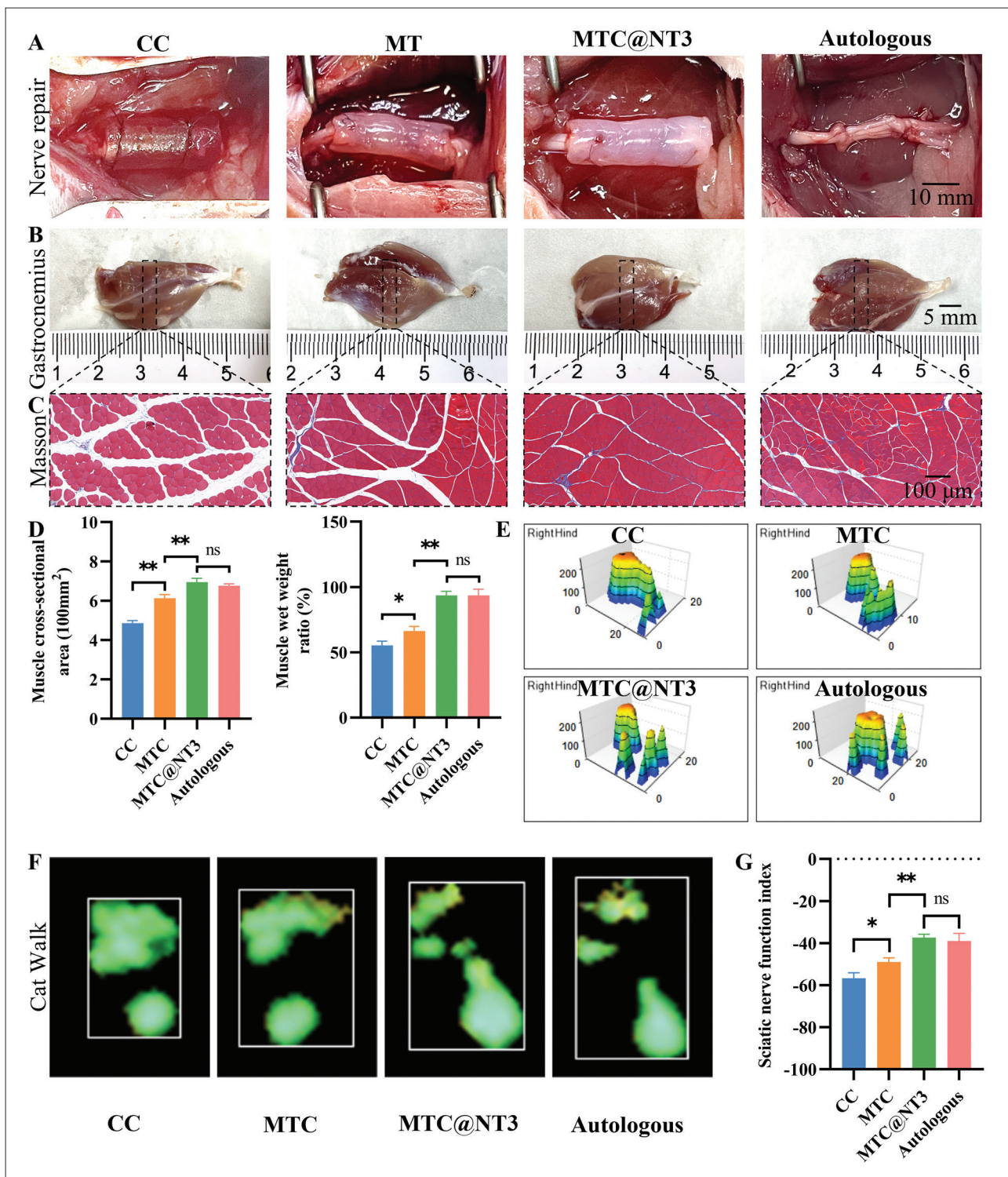
3.6. Gastrocnemius maintenance
As shown in **Figure S5** (Supplementary File), the complete degradation of CC and MTC took more than 36 weeks, enough time to support the reinnervation of the regenerated nerve to the target muscle. The rat gastrocnemius muscle was collected, weighed, and Masson-stained 8 weeks after the implantation surgery to verify the maintenance effect of different materials on the target organ[54]. As shown in Figure 5A, we induced a 15-mm long-distance sciatic nerve injury model in SD rats and repaired them with CC, MTC, MTC@NT3, and Autologous, respectively, and the MTC and MTC@NT3 groups had higher muscle cross-sectional area and wet weight than the CC group (Figure 5D). This is also consistent with the results in Figure 5B and C. We

hypothesized that the nerve conduit with tracks could promote faster regeneration of the severed sciatic nerve, thus achieving reinnervation of the putative muscle earlier and further serving to maintain the appearance and morphology of the target muscle. In week 12, we can see a similar pattern (**Figure S6** in Supplementary File). To further demonstrate that CC with MTC does not cause excessive inflammation, we performed HE staining and TNF-α immunofluorescence staining of the surrounding tissue 1 week after subcutaneous implantation (**Figure S7** in Supplementary File), which showed no significant difference between the CC and MTC groups (**Figure S8** in Supplementary File). As an important target organ of the sciatic nerve, maintaining the condition of the gastrocnemius muscle often affects functional recovery. Muscle wet weight, cross-sectional area, and muscle fiber density are the indicators of muscle status. MTC and MTC@NT3 can better maintain target muscle size and lay the foundation for functional recovery after nerve reinnervation.

3.7. Functional evaluation of regenerative nerves
To further evaluate how well MTC promotes functional recovery, we used the CatWalk instrument to analyze plantar pressures and footprints in model rats[55]. Although the MTC@NT3 and MTC groups had significantly improved function compared to the CC group, there were still differences compared to the uninjured sham group (Figure 5E and F). As shown in Figure 5G, SFI was better in the MTC@NT3 group compared with the MTC and CC groups, suggesting that MTC@NT3 effectively promoted functional recovery in the 15-mm sciatic nerve injury model in SD rats. We can conclude that the targeted guidance of MTC and the release of NT-3 factor enhance the regeneration of the sciatic nerve.

Three-dimensional printing technology has been widely used in the field of tissue engineering and regenerative medicine to create custom-made scaffolds that can support the growth and differentiation of cells. The scaffolds are designed to mimic the structure and function of natural tissues, providing a framework for new tissue growth and regeneration[56–60]. PNI is a common problem that can lead to the loss of motor and sensory function. Regenerating damaged peripheral nerves is a major challenge in the field of regenerative medicine[15,61–63]. One promising approach is to use neurotrophic factors, such as neurotrophin-3 (NT-3), which promotes nerve growth and regeneration[64–68]. Chitosan is a natural polysaccharide widely used as a biomaterial in tissue engineering and regenerative medicine. It has been shown to have excellent biocompatibility and biodegradability, making it an ideal material for scaffold fabrication and other biomedical applications[69–72]. Recent studies have investigated the

Figure 5. Functional effects of CC, MTC, MTC@NT3, and Autologous repair of peripheral nerves. (A) SD rat 15-mm long-distance defect model. (B) Observation of gastrocnemius maintenance. (C) Gastrocnemius muscle underwent Masson staining. (D) Gastrocnemius muscle cross-sectional area and wet weight in respective groups. (E) Pressure pattern map of the foot after repair of the rat nerve injury model. (F) Footprint map of the rat nerve injury model after repair. (G) Statistical map of sciatic nerve function index (ns = not significant, *$P < 0.05$, **$P < 0.01$).
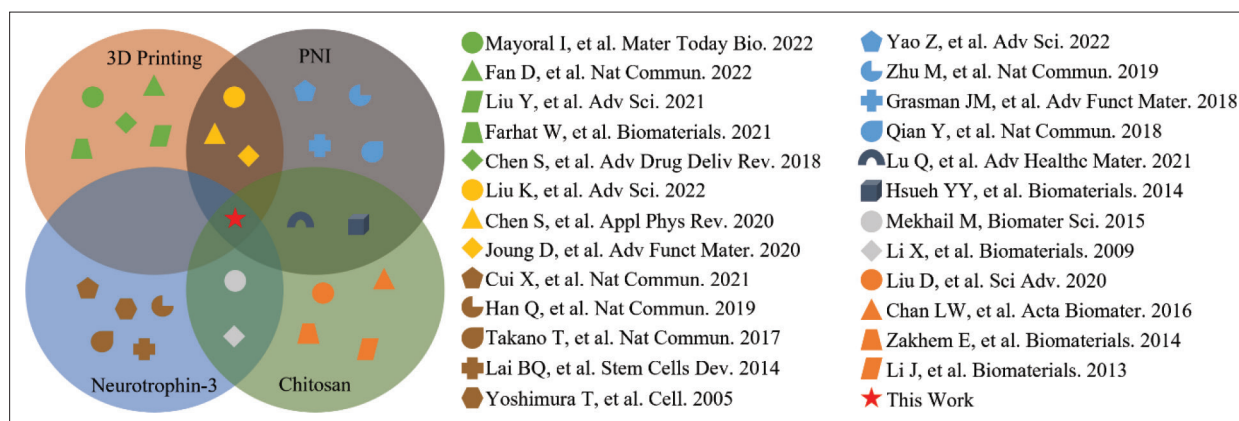
Figure 6. This work compares with studies related to 3D printing, NT-3, chitosan, and peripheral nerve injury.

application of chitosan scaffolds to promote peripheral nerve regeneration after injury. Researchers found that chitosan scaffolds implanted in rats with sciatic nerve injury significantly improved nerve regeneration and functional recovery[73,74]. Other studies have investigated the application of chitosan scaffolds loaded with NT-3 to promote nerve regeneration after injury. The results showed that chitosan scaffolds loaded with NT-3 significantly improved nerve regeneration and functional recovery compared to scaffolds without NT-3[75,76]. These studies suggest that by combining the unique properties of chitosan with NT-3 with the advantages of 3D printing technology, researchers may be able to create customized scaffolds that support nerve growth and regeneration in a targeted and effective manner[77–79]. The combination of 3D printing, PNI, NT-3, and chitosan holds great promise for developing effective therapies for nerve injury and other tissue regeneration applications. Overall, this work combined the potential of these technologies and optimized their use in clinical applications (Figure 6).

4. Conclusion

In conclusion, we successfully prepared a bionic microenvironmental neuroprosthetic conduit with 10–30 μm tracks to synergistically promote peripheral nerve regeneration using 3D printing topography technology and biological drug delivery. The prepared conduit with intact and stable micron structure and neural factors not only has good potential for peripheral nerve regeneration with good properties of inducing directional growth of Schwann cells, but also significantly promotes the regeneration and functional recovery of axons. The channels on MTC serve as a physical guide for the regeneration of axons, which are the lengthy extensions of nerve cells responsible for transmitting electrical signals. By creating a path for axonal growth and aligning them, the MTC can facilitate the healing of damaged or severed nerves. Research

has demonstrated that the MTC can promote nerve regeneration in both *in vitro* and *in vivo* models. Apart from providing a physical template, the MTC also has a role in regulating the local microenvironment. The MTC can bridge the gap between the two ends of a severed nerve and act as a conduit for the delivery of growth factors and other biomolecules that further enhance nerve regeneration. MTC will provide an important reference for the construction of peripheral nerve regeneration conduits with both physical effects (3D topography) and chemical effects (factors-loading). This study is expected to provide an important experimental and theoretical basis for the design of functional artificial neural implants.

Conflict of interest

The authors declare no conflicts of interest.

Author contributions

Conceptualization: Meng Zhang, Heng An

Formal analysis: Meng Zhang
Investigation: Pei-Xun Zhang, Yong-Qiang Wen, Ming Yang
Methodology: Teng Wan, Hao-Ran Jiang
Writing – original draft: Meng Zhang
Writing – review & editing: Meng Zhang, Heng An

Ethics approval and consent to participate

All animal use protocols in this study were approved by the Medical Ethics Committee of Peking University People's Hospital (approval number: 2022PHE078).

Consent for publication

Not applicable.

Availability of data

Not applicable.

References

1. Houdek MT, Shin AY, 2015, Management and complications of traumatic peripheral nerve injuries. *Hand Clin*, 31(2): 151–63.

   https://doi.org/10.1016/j.hcl.2015.01.007

2. Taylor CA, Braza D, Rice JB, *et al.*, 2008, The incidence of peripheral nerve injury in extremity trauma. *Am J Phys Med Rehabil*, 87(5): 381–385.

   https://doi.org/10.1097/PHM.0b013e31815e6370

3. Grijalvo S, Díaz DD, 2021, Graphene-based hybrid materials as promising scaffolds for peripheral nerve regeneration. *Neurochem Int*, 147: 105005.

   https://doi.org/10.1016/j.neuint.2021.105005

4. Yi S, Xu L, Gu X, 2019, Scaffolds for peripheral nerve repair and reconstruction. *Exp Neurol,* 319: 112761.

   https://doi.org/10.1016/j.expneurol.2018.05.016

5. Yin G, Peng Y, Lin Y, *et al.*, 2021, Long non-coding RNA MSTRG.24008.1 regulates the regeneration of the sciatic nerve via the miR-331-3p-NLRP3/MAL axis. *Front Cell Dev Biol*, 9: 641603.

   https://doi.org/10.3389/fcell.2021.641603

6. Bombeiro AL, Santini JC, Thomé R, *et al.*, 2016, Enhanced immune response in immunodeficient mice improves peripheral nerve regeneration following axotomy. *Front Cell Neurosci*, 10: 151.

   https://doi.org/10.3389/fncel.2016.00151

7. Jiang H, Wang X, Li X, *et al.*, 2022, A multifunctional ATP-generating system by reduced graphene oxide-based scaffold repairs neuronal injury by improving mitochondrial function and restoring bioelectricity conduction. *Mater Today Bio,* 13: 100211.

   https://doi.org/10.1016/j.mtbio.2022.100211

8. Mendes PM, 2008, Stimuli-responsive surfaces for bio-applications. *Chem Soc Rev*, 37(11): 2512–2529.

   https://doi.org/10.1039/b714635n

9. Zhu L, Jia S, Liu T, *et al.*, 2020, Aligned PCL fiber conduits immobilized with nerve growth factor gradients enhance and direct sciatic nerve regeneration. 30(39): 2002610.

   https://doi.org/10.1002/adfm.202002610

10. Houshyar S, Bhattacharyya A, Shanks R, 2019, Peripheral nerve conduit: Materials and Structures. *ACS Chem Neurosci,* 10(8): 3349–3365.

    https://doi.org/10.1021/acschemneuro.9b00203

11. Zhang J, Zhang X, Wang C, *et al.*, 2021, Conductive composite fiber with optimized alignment guides neural regeneration under electrical stimulation. 10(3): 2000604.

    https://doi.org/10.1002/adhm.202000604

12. Zhang X, Qu W, Li D, *et al.*, 2020, Functional polymer-based nerve guide conduits to promote peripheral nerve regeneration. *Adv Mater Interfaces*, 7(14): 2000225.

    https://doi.org/10.1002/admi.202000225

13. Gong B, Zhang X, Zahrani AA, *et al.*, 2022, Neural tissue engineering: From bioactive scaffolds and in situ monitoring to regeneration. *Exploration*, 2(3): 20210035.

    https://doi.org/10.1002/EXP.20210035

14. Li G, Li S, Zhang L, *et al.*, 2019, Construction of biofunctionalized anisotropic hydrogel micropatterns and their effect on schwann cell behavior in peripheral nerve regeneration. *ACS Appl Mater Interfaces*, 11(41): 37397–37410.

    https://doi.org/10.1021/acsami.9b08510

15. Grasman JM, Ferreira JA, Kaplan DL, 2018, Tissue models for neurogenesis and repair in 3D. *Adv Funct Mater*, 28(48): 1803822.

    https://doi.org/10.1002/adfm.201803822

16. Liu C, Chan C, 2016, An approach to enhance alignment and myelination of dorsal root ganglion neurons. *J Vis Exp,* (114): 54085.

    https://doi.org/10.3791/54085

17. Jia Y, Yang W, Zhang K, *et al.*, 2019, Nanofiber arrangement regulates peripheral nerve regeneration through differential modulation of macrophage phenotypes. *Acta Biomater*, 83: 291–301.

    https://doi.org/10.1016/j.actbio.2018.10.040

18. Hoffman-Kim D, Mitchel JA, Bellamkonda RV, 2010, Topography, cell response, and nerve regeneration. *Annu Rev Biomed Eng*, 12: 203–231.

    https://doi.org/10.1146/annurev-bioeng-070909-105351

19. Huang C, Ouyang Y, Niu H, *et al.*, 2015, Nerve guidance conduits from aligned nanofibers: Improvement of nerve

regeneration through longitudinal nanogrooves on a fiber surface. *ACS Appl Mater Interfaces*, 7(13): 7189–7196.

https://doi.org/10.1021/am509227t

20. Zhang Y, Xu Y, Kong H, *et al.*, 2023, Microneedle system for tissue engineering and regenerative medicine. *Exploration*, 3(1): 20210170.

https://doi.org/10.1002/EXP.20210170

21. Liu K, Yan L, Li R, *et al.*, 3D printed personalized nerve guide conduits for precision repair of peripheral nerve defects. *Adv Sci*, 9(12): 2103875.

https://doi.org/10.1002/advs.202103875

22. Ding J, Zhang J, Li J, *et al.*, 2019, Electrospun polymer biomaterials. *Prog Polym Sci,* 90: 1–34.

https://doi.org/10.1016/j.progpolymsci.2019.01.002

23. Wan X, Zhao Y, Li Z, *et al.*, 2022, Emerging polymeric electrospun fibers: From structural diversity to application in flexible bioelectronics and tissue engineering. *Exploration*, 2(1): 20210029.

https://doi.org/10.1002/EXP.20210029

24. Zhao C, Wang X, Gao L, *et al.*, 2018, The role of the micro-pattern and nano-topography of hydroxyapatite bioceramics on stimulating osteogenic differentiation of mesenchymal stem cells. *Acta Biomater*, 73: 509–521.

https://doi.org/10.1016/j.actbio.2018.04.030

25. Mansouri N, Bagheri S, 2016, The influence of topography on tissue engineering perspective. *Mater Sci Eng C Mater Biol Appl*, 61: 906–921.

https://doi.org/10.1016/j.msec.2015.12.094

26. Klymov A, Rodrigues Neves CT, te Riet J, *et al.*, 2015, Nanogrooved surface-patterns induce cellular organization and axonal outgrowth in neuron-like PC12-cells. *Hear Res,* 320: 11–17.

https://doi.org/10.1016/j.heares.2014.12.009

27. Zhang D, Yao Y, Duan Y, *et al.*, 2020, Surface-anchored graphene oxide nanosheets on cell-scale micropatterned poly(d,l-lactide-co-caprolactone) conduits promote peripheral nerve regeneration. *ACS Appl Mater Interfaces,* 12(7): 7915–7930.

https://doi.org/10.1021/acsami.9b20321

28. Omidinia-Anarkoli A, Ephraim JW, Rimal R, *et al.*, 2020, Hierarchical fibrous guiding cues at different scales influence linear neurite extension. *Acta Biomater*, 113: 350–359.

https://doi.org/10.1016/j.actbio.2020.07.014

29. Li G, Zheng T, Wu L, *et al.*, 2021, Bionic microenvironment-inspired synergistic effect of anisotropic micro-nanocomposite topology and biology cues on peripheral nerve regeneration. *Sci Adv*, 7(28): 5812.

https://doi.org/10.1126/sciadv.abi5812

30. Li G, Zhao X, Zhang L, *et al.*, 2014, Regulating Schwann cells growth by chitosan micropatterning for peripheral nerve regeneration in vitro. *Macromol Biosci*, 14(8): 1067–1075.

https://doi.org/10.1002/mabi.201400098

31. Iadecola C, 2010, The overlap between neurodegenerative and vascular factors in the pathogenesis of dementia. *Acta Neuropathol,* 120(3): 287–296.

https://doi.org/10.1007/s00401-010-0718-6

32. Martínez G, Khatiwada S, Costa-Mattioli M, *et al.*, 2018, ER proteostasis control of neuronal physiology and synaptic function. *Trends Neurosci*, 41(9): 610–624.

https://doi.org/10.1016/j.tins.2018.05.009

33. Wang T, Zhong X, Wang S, *et al.*, 2012, Molecular mechanisms of RADA16-1 peptide on fast stop bleeding in rat models. *Int J Mol Sci*, 13(11): 15279–15290.

https://doi.org/10.3390/ijms131115279

34. Hu G, Xiao L, Tong P, *et al.*, 2012, Antibacterial hemostatic dressings with nanoporous bioglass containing silver. *Int J Nanomed,* 7: 2613–2620.

https://doi.org/10.2147/ijn.S31081

35. Dong H, Li Z, Bian S, *et al.*, 2022, Culture of patient-derived multicellular clusters in suspended hydrogel capsules for pre-clinical personalized drug screening. *Bioact Mater*, 18: 164–177.

https://doi.org/10.1016/j.bioactmat.2022.03.020

36. Yu X, Zhu D, Luo B, *et al.*, 2022, IFNγ enhances ferroptosis by increasing JAK-STAT pathway activation to suppress SLCA711 expression in adrenocortical carcinoma. *Oncol Rep,* 47(5): 97.

https://doi.org/10.3892/or.2022.8308

37. Nika MC, Ntaiou K, Elytis K, *et al.*, 2020, Wide-scope target analysis of emerging contaminants in landfill leachates and risk assessment using Risk Quotient methodology. *J Hazard Mater,* 394: 122493.

https://doi.org/10.1016/j.jhazmat.2020.122493

38. Xia W, Zhu J, Wang X, *et al.*, 2020, Overexpression of Foxc1 regenerates crushed rat facial nerves by promoting Schwann cells migration via the Wnt/β-catenin signaling pathway. *J Cell Phys,* 235(12): 9609–9622.

https://doi.org/10.1002/jcp.29772

39. Rao F, Wang Y, Zhang D, *et al.*, 2020, Aligned chitosan nanofiber hydrogel grafted with peptides mimicking bioactive brain-derived neurotrophic factor and vascular endothelial growth factor repair long-distance sciatic nerve defects in rats. *Theranostics*, 10(4): 1590–1603.

https://doi.org/10.7150/thno.36272

40. Torres-Mejía E, Trümbach D, Kleeberger C, *et al.*, 2020, Sox2 controls Schwann cell self-organization through fibronectin fibrillogenesis. *Sci Rep*, 10(1): 1984.

https://doi.org/10.1038/s41598-019-56877-y

41. Riggio C, Calatayud MP, Hoskins C, *et al.*, 2012, Poly-l-lysine-coated magnetic nanoparticles as intracellular actuators for neural guidance. *Int J Nanomed,* 7: 3155–3166.

https://doi.org/10.2147/ijn.S28460

42. Cai J, Peng X, Nelson KD, *et al.*, 2005, Permeable guidance channels containing microfilament scaffolds enhance axon growth and maturation. *J Biomed Mater Res A*, 75(2): 374–386.

https://doi.org/10.1002/jbm.a.30432

43. Puhl DL, Funnell JL, D'Amato AR, *et al.*, 2020, Aligned fingolimod-releasing electrospun fibers increase dorsal root ganglia neurite extension and decrease schwann cell expression of promyelinating factors. *Front Bioeng Biotechnol*, 8: 937.

https://doi.org/10.3389/fbioe.2020.00937

44. Morano M, Wrobel S, Fregnan F, *et al.*, 2014, Nanotechnology versus stem cell engineering: In vitro comparison of neurite inductive potentials. *Int J Nanomed,* 9: 5289–5306.

https://doi.org/10.2147/ijn.S71951

45. Li M, Tang Z, Lv S, *et al.*, 2014, Cisplatin crosslinked pH-sensitive nanoparticles for efficient delivery of doxorubicin. *Biomaterials*, 35(12): 3851–3864.

https://doi.org/10.1016/j.biomaterials.2014.01.018

46. Cao F, Ju E, Zhang Y, *et al.*, 2017, An efficient and benign antimicrobial depot based on silver-infused MoS(2). *ACS Nano*, 11(5): 4651–4659.

https://doi.org/10.1021/acsnano.7b00343

47. Xu Y, Zhou J, Liu C, *et al.*, 2021, Understanding the role of tissue-specific decellularized spinal cord matrix hydrogel for neural stem/progenitor cell microenvironment reconstruction and spinal cord injury. *Biomaterials*, 268: 120596.

https://doi.org/10.1016/j.biomaterials.2020.120596

48. Alvarsson A, Jimenez-Gonzalez M, Li R, *et al.*, 2020, A 3D atlas of the dynamic and regional variation of pancreatic innervation in diabetes. *Sci Adv*, 6(41): 9124.

https://doi.org/10.1126/sciadv.aaz9124

49. Asbury AK, King RH, Reilly MM, *et al.*, 2011, Professor P. K. Thomas: clinician, investigator, editor and leader--a retrospective appreciation. *Brain*, 134(Pt 2): 618–626.

https://doi.org/10.1093/brain/awq230

50. Afshari FT, Kwok JC, White L, *et al.*, 2010, Schwann cell migration is integrin-dependent and inhibited by astrocyte-produced aggrecan. *Glia*, 58(7): 857–869.

https://doi.org/10.1002/glia.20970

51. Benoy V, Van Helleputte L, Prior R, *et al.*, 2018, HDAC6 is a therapeutic target in mutant GARS-induced Charcot-Marie-Tooth disease. *Brain*, 141(3): 673–687.

https://doi.org/10.1093/brain/awx375

52. Hu H, Jonas P, 2014, A supercritical density of Na(+) channels ensures fast signaling in GABAergic interneuron axons. *Nat Neurosci,* 17(5): 686–693.

https://doi.org/10.1038/nn.3678

53. Eichel MA, Gargareta VI, D'Este E, *et al.*, 2020, CMTM6 expressed on the adaxonal Schwann cell surface restricts axonal diameters in peripheral nerves. *Nat Commun*, 11(1): 4514.

https://doi.org/10.1038/s41467-020-18172-7

54. Wang L, Lu C, Yang S, *et al.*, 2020, A fully biodegradable and self-electrified device for neuroregenerative medicine. *Sci Adv*, 6(50): 6686.

https://doi.org/10.1126/sciadv.abc6686

55. Jin B, Yu Y, Chen X, *et al.,* 2023, Microtubes with gradient decellularized porcine sciatic nerve matrix from microfluidics for sciatic nerve regeneration. *Bioact Mater*, 21: 511–519.

https://doi.org/10.1016/j.bioactmat.2022.08.027

56. Mayoral I, Bevilacqua E, Gómez G, *et al.,* 2022, Tissue engineered in-vitro vascular patch fabrication using hybrid 3D printing and electrospinning. *Mater Today Bio,* 14: 100252.

https://doi.org/10.1016/j.mtbio.2022.100252

57. Fan D, Yuan X, Wu W, *et al.*, 2022, Self-shrinking soft demoulding for complex high-aspect-ratio microchannels. *Nat Commun*, 13(1): 5083.

https://doi.org/10.1038/s41467-022-32859-z

58. Liu Y, Dabrowska C, Mavousian A, *et al.*, 2021, Bio-assembling macro-scale, lumenized airway tubes of defined shape via multi-organoid patterning and fusion. *Adv Sci,* 8(9): 2003332.

https://doi.org/10.1002/advs.202003332

59. Farhat W, Chatelain F, Marret A, *et al.*, 2021, Trends in 3D bioprinting for esophageal tissue repair and reconstruction. *Biomaterials*, 267: 120465.

https://doi.org/10.1016/j.biomaterials.2020.120465

60. Chen S, Li R, Li X, *et al.*, 2018, Electrospinning: An enabling nanotechnology platform for drug delivery and regenerative medicine. *Adv Drug Deliv Rev*, 132: 188–213.

https://doi.org/10.1016/j.addr.2018.05.001

61. Yao Z, Yuan W, Xu J, *et al.*, 2022, Magnesium-encapsulated injectable hydrogel and 3D-engineered polycaprolactone conduit facilitate peripheral nerve regeneration. *Adv Sci,* 9(21): e2202102.

https://doi.org/10.1002/advs.202202102

62. Zhu M, Li W, Dong X, *et al.*, 2019, In vivo engineered extracellular matrix scaffolds with instructive niches for oriented tissue regeneration. *Nat Commun*, 10(1): 4620.

https://doi.org/10.1038/s41467-019-12545-3

63. Qian Y, Zhao X, Han Q, *et al.*, 2018, An integrated multi-layer 3D-fabrication of PDA/RGD coated graphene loaded PCL nanoscaffold for peripheral nerve restoration. *Nat Commun*, 9(1): 323.

https://doi.org/10.1038/s41467-017-02598-7

64. Cui X, Jing J, Wu R, *et al.*, 2021, Adipose tissue-derived neurotrophic factor 3 regulates sympathetic innervation and thermogenesis in adipose tissue. *Nat Commun*, 12(1): 5362.

https://doi.org/10.1038/s41467-021-25766-2

65. Han Q, Ordaz JD, Liu NK, *et al.*, 2019, Descending motor circuitry required for NT-3 mediated locomotor recovery after spinal cord injury in mice. *Nat Commun*, 10(1): 5815.

https://doi.org/10.1038/s41467-019-13854-3

66. Takano T, Wu M, Nakamuta S, *et al.*, 2017, Discovery of long-range inhibitory signaling to ensure single axon formation. *Nat Commun*, 8(1): 33.

https://doi.org/10.1038/s41467-017-00044-2

67. Lai BQ, Wang JM, Ling EA, *et al.*, 2014, Graft of a tissue-engineered neural scaffold serves as a promising strategy to restore myelination after rat spinal cord transection. *Stem Cells Dev*, 23(8): 910–921.

https://doi.org/10.1089/scd.2013.0426

68. Yoshimura T, Kawano Y, Arimura N, *et al.,* 2005, GSK-3beta regulates phosphorylation of CRMP-2 and neuronal polarity. Cell, 120(1): 137–149:.

https://doi.org/10.1016/j.cell.2004.11.012

69. Liu D, Shu G, Jin F, *et al.*, 2020, ROS-responsive chitosan-SS31 prodrug for AKI therapy via rapid distribution in the kidney and long-term retention in the renal tubule. *Sci Adv*, 6(41): 7422.

https://doi.org/10.1126/sciadv.abb7422

70. Chan LW, Kim CH, Wang X, *et al.*, 2016, PolySTAT-modified chitosan gauzes for improved hemostasis in external hemorrhage. *Acta Biomater*, 31: 178–185.

https://doi.org/10.1016/j.actbio.2015.11.017

71. Zakhem E, Raghavan S, Bitar KN, 2014, Neo-innervation of a bioengineered intestinal smooth muscle construct around chitosan scaffold. *Biomaterials*, 35(6): 1882–1889.

https://doi.org/10.1016/j.biomaterials.2013.11.049

72. Li J, Shu Y, Hao T, *et al.*, 2013, A chitosan-glutathione based injectable hydrogel for suppression of oxidative stress damage in cardiomyocytes. *Biomaterials*, 34(36): 9071–9081.

https://doi.org/10.1016/j.biomaterials.2013.08.031

73. Lu Q, Zhang F, Cheng W, *et al.*, 2021, Nerve guidance conduits with hierarchical anisotropic architecture for peripheral nerve regeneration. *Adv Healthc Mater*, 10(14): e2100427.

https://doi.org/10.1002/adhm.202100427

74. Hsueh YY, Chang YJ, Huang TC, *et al.*, 2014, Functional recoveries of sciatic nerve regeneration by combining chitosan-coated conduit and neurosphere cells induced from adipose-derived stem cells. *Biomaterials*, 35(7): 2234–2244.

https://doi.org/10.1016/j.biomaterials.2013.11.081

75. Mekhail M, Almazan G, Tabrizian M, 2015, Purine-crosslinked injectable chitosan sponges promote oligodendrocyte progenitor cells' attachment and differentiation. *Biomater Sci*, 3(2): 279–287.

https://doi.org/10.1039/c4bm00215f

76. Li X, Yang Z, Zhang A, 2009, The effect of neurotrophin-3/chitosan carriers on the proliferation and differentiation of neural stem cells. *Biomaterials*, 30(28): 4978–4985.

https://doi.org/10.1016/j.biomaterials.2009.05.047

77. Liu K, Yan L, Li R, *et al.*, 2022, 3D printed personalized nerve guide conduits for precision repair of peripheral nerve defects. *Adv Sci*, 9(12): e2103875.

https://doi.org/10.1002/advs.202103875

78. Chen S, John JV, McCarthy A, *et al.*, 2020, Fast transformation of 2D nanofiber membranes into pre-molded 3D scaffolds with biomimetic and oriented porous structure for biomedical applications. *Appl Phys Rev,* 7(2): 021406.

https://doi.org/10.1063/1.5144808

79. Joung D, Lavoie NS, Guo SZ, *et al.*, 2020, 3D printed neural regeneration devices. *Adv Funct Mater*, 30(1): 10.

https://doi.org/10.1002/adfm.201906237